LA-UR- 02-2468 *c.1*

Title: | "CORROSION RATES FOR NICKEL BASED ALLOYS C276 AND 625 AS A FUNCTION OF PROTON BEAM CURRENT"

Author(s): | Scott Lillard

Submitted to:

LOS ALAMOS NATIONAL LABORATORY

3 9338 01054 3964

Los Alamos
NATIONAL LABORATORY

Los Alamos

NATIONAL LABORATORY

memorandum

Materials Science and Technology Division

MST-6, Metallurgy Section , MS G755
Los Alamos, New Mexico 87545

To: Frank Gac
MS: MS H809
From/Group/MS: Scott Lillard/MST-6/G755
Phone/FAX/:email 7-6325/7-2264/lillard@lanl.gov
Symbol: MST-6-00-033
Date: June 6, 2000

SUBJECT: Corrosion Rates for Nickel based Alloys C276 and 625 as a Function of Proton Beam Current

This memo addresses the effects of proton beam current and sample location on the corrosion rate of nickel based alloys C276 (UNS N10276) and 625 (UNS N06625). The data presented here were collected in the corrosion loop at the LANSCE A6 target station during the period between October 10 and October 14, 1998. During this period only the corrosion loop was in-beam, no other inserts were between the corrosion loop and the UHV window. Nominally, the proton beam energy was 800 MeV and the average beam current was varied between 0.010 and 0.34 mA. Specific proton beam parameters can be found in previous memos (MST-6-99-039). The relative position of these probes with respect to the proton beam are presented in Figure 1. A description of the probe design and how the probes were fabricated has been addressed in earlier publications.
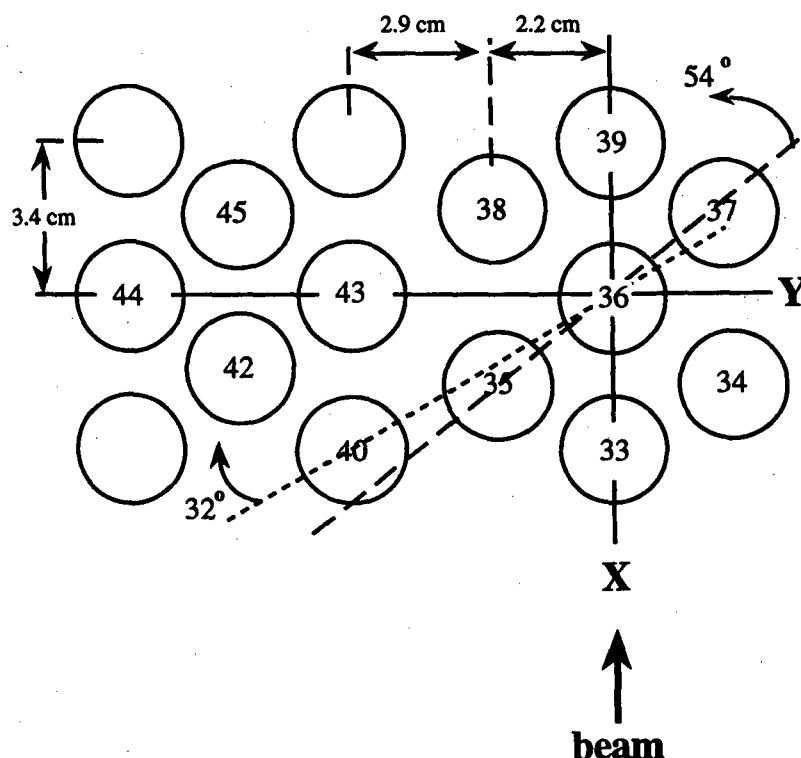

Figure 1 A perspective of the tube array irradiated during the FY '99 irradiation at the LANSCE A6 target station from the front, top-down. Two tubes contained nickel based corrosion samples: tubes 34 and 37 (alloys 625 and C276 respectively). The path of the proton beam was parallel to the X axis at Y=0. Here we have arbitrarily defined tube 36 as (0,0), the manifold center.

Prior to operation, the corrosion loop was thoroughly cleaned and flushed with DI water. The system was then filled with DI water for operation. The dissolved hydrogen concentration in the water system, obtained by continuously bubbling Ar 6%-H_2 into the system, was approximately 0.4 ppm prior to irradiation. The hydrogen concentration measured during proton irradiation was 2-3 ppm. This increase during proton irradiation is believed to owe to water radiolysis. The water resistivity at the beginning of this irradiation period was approximately 1.2 MΩ·cm. By the end of this irradiation period the resistivity had decreased to approximately 0.035 MΩ·cm. These parameters are only a few of those relevant to the investigation and are presented for clarity. A thorough discussion of these parameters will be presented in future publications.

All corrosion rates reported here were calculated from electrochemical impedance spectroscopy (EIS) data. EIS data were collected with a floating ground system in the traditional three electrode configuration where one of the corrosion probes served as the reference electrode and the stainless steel water system served as the counter electrode. Typical Bode magnitude and phase plots from EIS data for alloy 625 (tube 34) at a beam current of 0.10 mA are presented in Figure 2. Similar results were obtained for alloy C276. To obtain polarization resistance (R_{pol}) from the data, complex non-linear least squares (CNLS) fitting was employed. As can be seen in Figure 2, a single time constants was observed in the data (single minima in the phase data). The equivalent circuit (EC) used to model the data in CNLS fitting is presented in Figure 3. This EC is a parallel resistor/capacitor (RC) circuit in series with a resistive element where: R_{pol} is the polarization resistance, cpe is a constant phase element, and R_{sol} is the geometric solution resistance between the sample and the reference electrode.
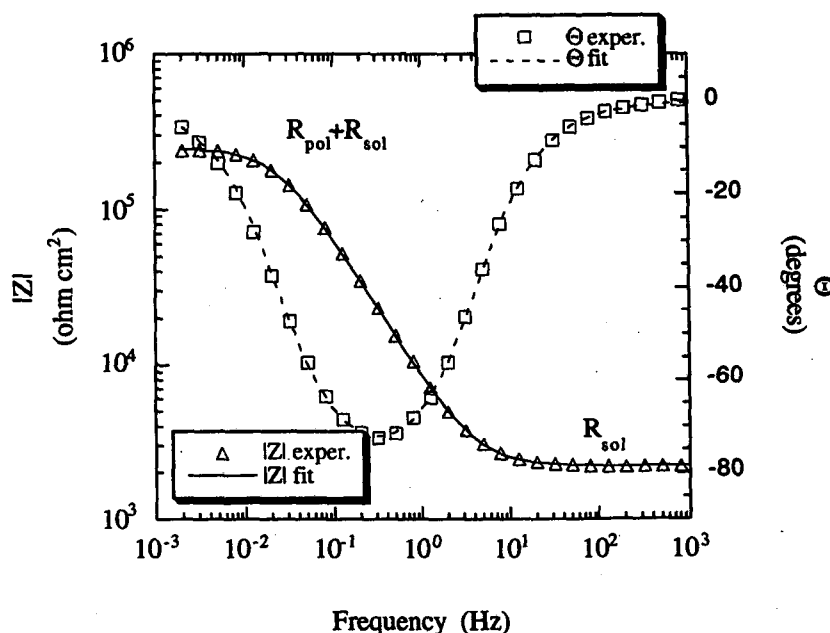
Figure 2 Bode magnitude and phase plots for alloy 625 in tube 34 during proton irradiation at 0.10 mA. For clarity, only every other experimental data point is shown.
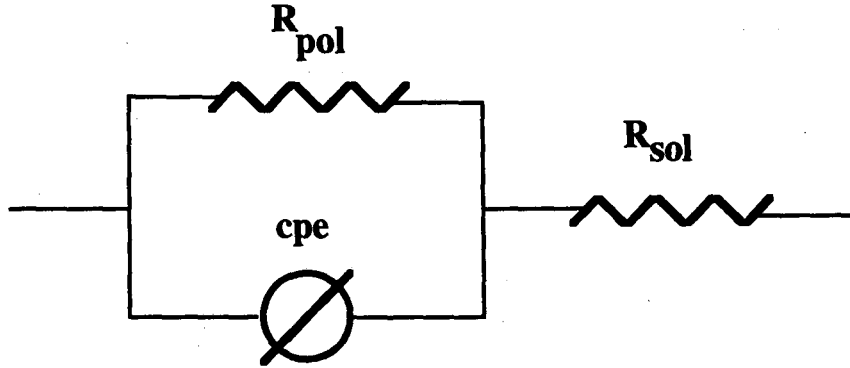
Figure 3 Equivalent circuit used to model the EIS data for both alloy 625 and alloy C276. Where: R_{pol} is the polarization resistance, cpe is a constant phase element, and R_{sol} is the geometric solution resistance between the sample and the reference electrode.

A fit of the model to the experimental data is shown in Figure 2 as solid and dashed lines. As can be seen, excellent agreement between the model and the data exists. It may be noted that the EC shown in Figure 3 assumes that no localized corrosion (pitting corrosion) is-occurring on the sample surface. Given that the experiments were conducted in DI water and the excellent pitting resistance of both alloys even in concentrated acidic chloride solutions this assumption should be valid. From the CNLS modeling of the data, R_{pol} was determined by subtracting the value of $|Z|$ at high frequency (equal to R_{sol}) from the value of $|Z|$ at low frequency (equal to $R_{pol}+R_{sol}$). R_{pol} is then used to determine corrosion rate.

Uniform corrosion rates in μm/year of irradiation ($CR_{\mu m/yr.}$) were calculated from R_{pol} and the well know expression:

$$CR_{\mu m/yr.} = \frac{129 \cdot 25.4\left(\left(0.026/R_{pol}\right)1000\right)(EW)}{\rho} \qquad (1)$$

where: R_{pol} is the uniform polarization resistance normalized for total area (in ohm•cm^2), EW is equivalent weight and is equal to 27.09 and 25.01 (unitless) for C276 and 625 respectively, and ρ is density and is equal to 8.89 g/cm^3 and 8.44 g/cm^3 for C276 and 625 respectively Table 2 summarizes the uniform corrosion rate results. As observed for the in-beam Alloy 718 (MST-6-99-039) and stainless steel 316L (MST-6-99-089) corrosion probes, the increase in uniform corrosion rate of the nickel based alloy in each tube was nearly linear with increasing beam current (Figures 4 and 5):

alloy 625   log(CR)=1.11+1.22log(BC)   (2)

alloy C276   log(CR)=1.18+1.15log(BC)   (3)

where CR is corrosion rate in μm/year of irradiation and BC is the average beam current in mA. For comparison, the corrosion rates of SS 316L samples in similar locations (tubes 34 and 37) have been presented along with those results obtained for Alloys 625 and C276 in Figures 4 and 5. While it appears that the corrosion rates of the nickel base alloys were consistently lower than stainless steel for similar locations relative to the beam centerline, the calculated neutron (and photon) flux in the region of tubes 34 and 37 was lower than that in the region of tubes 35 and 38 (FIgure 6).

Table 1 Uniform corrosion rates for nickel base alloys in μm/year of irradiation as a function of proton beam current. See Figure 1 for tube location.

| tube # location (cm)	beam off	0.01 mA	0.036 mA	0.10 mA	0.34 mA
625 tube #34	0.005	0.062	0.117	1.02	3.60
C276 tube #37	0.01	0.094	0.199	1.30	4.52
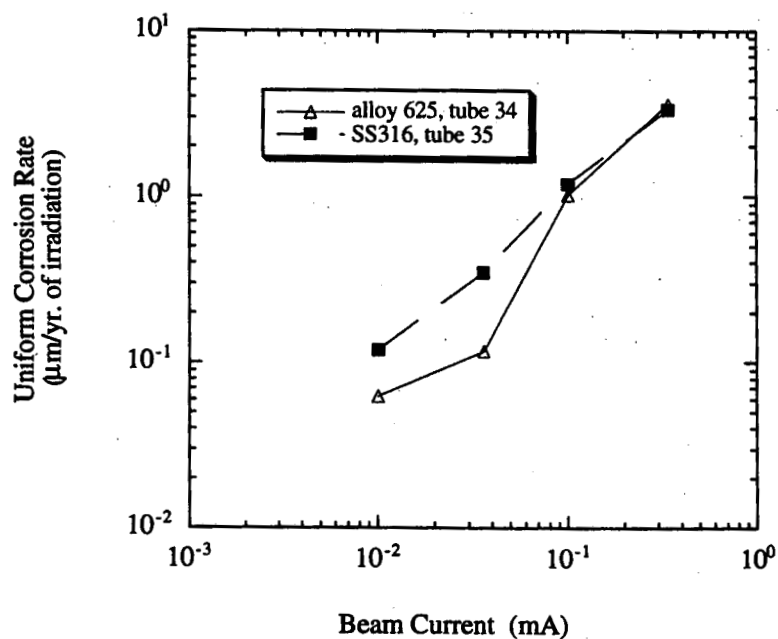
Figure 4 Uniform corrosion rates for per yr. of irradiation as a function of proton beam current for Alloy 625 in tube and SS 316L in tube (MST-6-99-089).
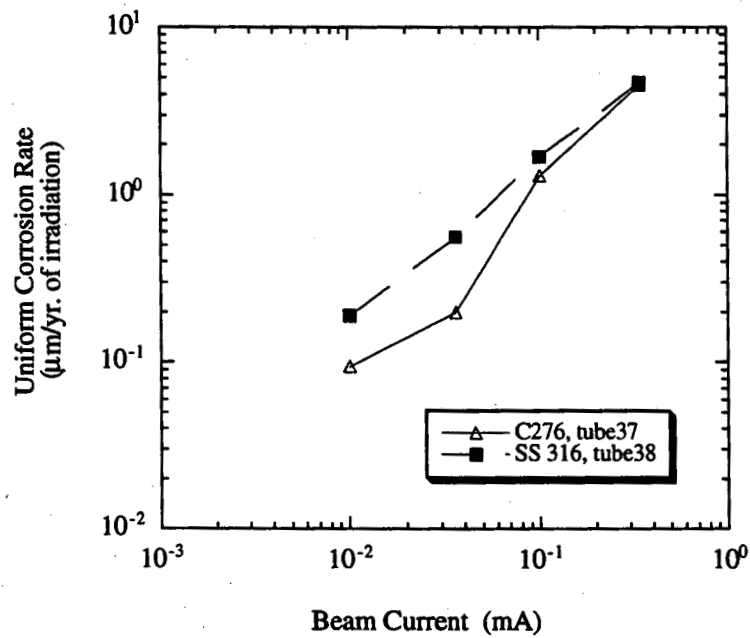
Figure 5 Uniform corrosion rates for alloy C276 (tube 37) per yr. of irradiation as a function of proton beam current. For comparison the corrosion rate of SS 316L (tube 38, MST-6-99-089) are also presented.
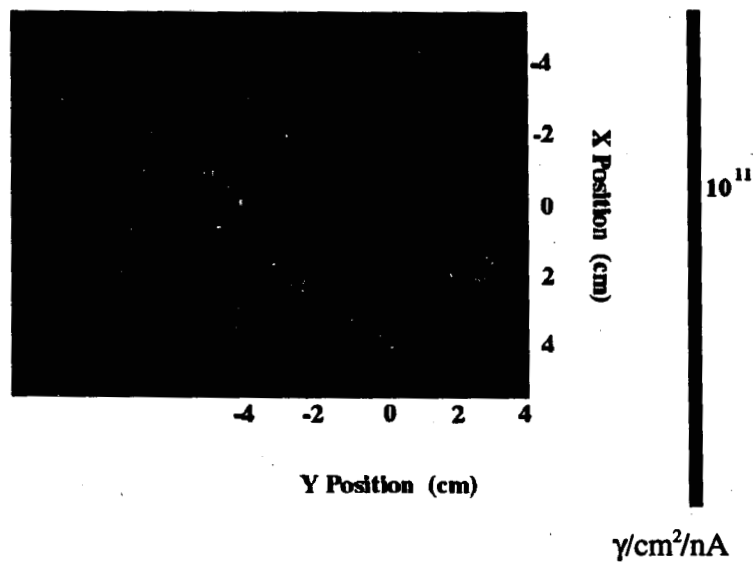
Figure 6 Neutron flux distribution for the corrosion insert from MCNPX transport calculations. A similar distribution was also observed for photons. Data were calculated with all other inserts removed from the proton beam. (from P. Ferguson LANSCE-12)

However, the magnitude of the proton flux was similar for the SS and nickel based corrosion probes. This suggests that a secondary particle such as neutrons, electrons, or photons is the primary factor in determining corrosion rate. This is consistent with the SS 316L data (MST-6-99-089) that showed the trend in corrosion rate with probe position was similar to the trend in photon and neutron distribution.

In conclusion, the results presented in this memo demonstrate that the uniform corrosion rates of nickel based alloys increased with proton beam current in a manner similar to that described for other alloys (Alloy 718: MST-6-99-039, 316L SS: MST-6-99-089, Al6061: MST-6-99-0149). While the corrosion rates of the nickel base alloys were consistently lower than stainless steel for similar locations relative to the beam centerline, the calculated neutron (and photon) flux in the region of tubes 34 and 37 was lower than that in the region of tubes 35 and 38. Therefore, although these alloys have greatly improved corrosion resistance over stainless steels in aggressive high chloride low pH environments, it does not appear that they offer a greatly improved resistance over 316L SS in radiation environments where deionized water is used as a coolant.

distribution list:

MST-6, G770
CIC-10, A150